# An elastic phenomenological material law of technical textile with a nonlinear shear behavior

Dániel T. Karádi

*Dept. Mechanics, Materials and Structures, Budapest University of Technology and Economics, Budapest, Hungary*

+36 1 463-1315

daniel.karadi@szt.bme.hu

www.szt.bme.hu

András A. Sipos

*Dept. Mechanics, Materials and Structures, Budapest University of Technology and Economics, Budapest, Hungary*

+36 1 463 2316

siposa@eik.bme.hu

www.szt.bme.hu

Marianna Halász

*Rejtő Sándor Faculty of Light Industry and Environmental Protection Engineering, Óbuda Univeristy, Budapest, Hungary*

**+36 1 666-5972**

halasz.marianna@rkk.uni-obuda.hu

Hliva Viktor

*Dept. Polymer Engineering, Budapest University of Technology and Economics, Budapest, Hungary*

+36 1 463 2650

hlivav@pt.bme.hu

www.pt.bme.hu

Dezső Hegyi

*Dept. Mechanics, Materials and Structures, Budapest University of Technology and Economics, Budapest, Hungary*

+36 1 463 2316

+36 1 463 1773

hegyi.dezso@szt.bme.hu

www.szt.bme.hu

**Abstract**

In technical textile engineering, macro-level phenomenological modeling effectively describes the material's highly nonlinear behavior. However, existing material laws concentrate on the normal stiffness in the orthotropic yarns and simplify the shear effect because of the two orders of magnitude difference between shear and normal stiffness. This paper introduces an improved phenomenological model that includes nonlinear shear behavior, and it determines the material parameters with a previously applied[1] data fitting method for exponential functions. The nonlinear shear behavior is valid for the elastic state, i.e., at the service level of the loads. Time-dependent, cyclic loading, or plastic behavior are not considered.

*Keywords: technical textiles, nonlinear constitutive law, uniaxial test, shear modulus*

# 1. Introduction

On the one hand, structural design requires precise and reliable material models. On the other hand, they should keep on being straightforward and effective, too, without any negligible or minor parameters. Woven technical textiles have significant geometric and material nonlinearities, which are still being treated differently from the micro- to the macro-levels.

This paper intends to improve a method published before[2], implementing a nonlinear elastic shear constitutive law for technical textiles.

Lomov and his group[3] created a complex 3D meso-level model of the yarns for simulating the macro-level behavior of the fabric. Haan and his group[4] developed a homogenized elastic model where the yarns of a one-layer textile are modeled like bars. Ballhouse and his group[5] took into consideration the time-dependent properties on the meso-level of the fabrics. Durville[6] constructed a meso-level structure with 3D beam elements for complex macro-level numerical simulations.

Still, these methods require detailed knowledge about the geometry at the meso-level of the textile in question. Therefore, they can hardly serve as a method for engineering purposes as their generalization on the textile structure's surface is challenging.

The following phenomenological models in the literature succeeded in capturing the nonlinear behavior solely on the macro level. The dense net method[7,8] uses two independent functions to be calibrated with the uniaxial measurements in the orthotropic directions; nonetheless, the model cannot handle the interaction phenomenon between the two yarn directions. The spline method[9,10] defines the surface for the stress as a function of the two orthogonal elongations using power series to characterize the spline. The method's main disadvantage is that it can lead to a divergent nonlinear analysis due to the behavior of power functions during extrapolation.

Some other methods use adequate nonlinear functions[11,12] to describe the textile behavior in the elastic range; however, they still consist of significant simplifications and computational uncertainties.

Numerous researchers[13–16] provide a continuum description for textile fabrics and characterize their behavior with some hyperelastic constitutive model. These models determine the stress tensor through the derivative of the strain energy density, which is formulated as a function of the strain invariants representative to the anisotropy of the deformed, initially orthotropic material. The strain invariants derived from structural tensors are identified with the help of the deformation modes of the fabric, i.e., they are based on physical observations[13].

Hegyi et al.[2], carried out short-time uniaxial and biaxial tension tests on PTFE-coated glass fibre woven textiles to describe macro-level coated textile behavior on the elastic range. In their new phenomenological model, they have eliminated the shortcomings described above. Their equations described the elongations of the orthogonal yarns with two exponential functions and a power function that

characterize the interaction between the yarns. In that model, the shear stiffness was simplified to a linear function.

Even though the presented macro and meso-level models capture the fabric behavior in detail, they are far too complicated or impractical for engineering usage. Some of them have too high computational and input parameter needs. Others neglect the interaction of the two orthotropic yarns. Finally, some methods can become numerically unstable at a nonlinear analysis of the membrane.

The present paper aims to capture the shear effect and update the existing phenomenological model with the shear stiffness for proper engineering usage. For the result, uniaxial tensile tests were carried out on PVC coated polyester-fiber textiles in different yarn-load directions.

# 2. The existing orthotropic elastic phenomenological material law

This Section briefly introduces the existing orthotropic elastic phenomenological material law developed by Hegyi et al.[2]. It is well known that the nonlinearity of the stress-strain function of the technical textiles comes from the straightening of the mostly linear elastic fibres during the loading. To capture this macroscopic behavior, the authors carried out three types of experimental series: uniaxial tensile tests in the two orthogonal yarn directions, and a biaxial tensile test on a crossed shape specimen, with the help of a special pulley system[17,18]. Engineering strains were measured on a 30 by 30 mm area at the center of the samples with a video extensometer. The used material was a PTFE coated woven glass fibre. In the present paper, PVC coated woven polyester fibre material is used. Table 1. contains the main parameters of the two materials for comparison.

**Table 1.** Comparison of the investigated materials

| Material | Verseidang Duraskin B 18089[2] | Sauleda Monza Polyester AT 1100 |
|---|---|---|
| Yarns | Glass fibre | Polyester |
| Weave type | Simple plain weave | Simple plain weave |
| Coating | PTFE | PVC |
| Average thickness [mm] | 0.67 | 0.48 |
| Surface density [$\frac{g}{mm^2}$] | 1150 | 580 |

### 2.1. Uniaxial behavior with the interaction of the yarns

The following two functions describe the normal stress-strain curve:

$$\sigma_w = a_1 \varepsilon_w \left(1 - e^{-a_3 \varepsilon_w^2}\right) + a_2 \varepsilon_w \left(e^{-a_4 \varepsilon_w^2}\right) + c_1 \varepsilon_f \left(\varepsilon_w^2 \varepsilon_f^2\right)^{c_2} \tag{1}$$

$$\sigma_f = b_1 \varepsilon_f \left(1 - e^{-b_3 \varepsilon_f^2}\right) + b_2 \varepsilon_f \left(e^{-b_4 \varepsilon_f^2}\right) + c_1 \varepsilon_w \left(\varepsilon_w^2 \varepsilon_f^2\right)^{c_2} \tag{2}$$

where $\sigma_w$ and $\sigma_f$ $[N/mm^2]$ are the engineering stress in the warp and weft direction, and $\varepsilon_w$ and $\varepsilon_f$ [%] denote the engineering strain in the warp and weft directions, respectively. The engineering stress measures the force applied to the material on the reference (stress free) area. For the engineering strain, the change in the length of a segment is divided by the reference length of the segment. Using the geometry of the reference state is utilized in the experimental tests (in eqs. 9 and 10). In the formula of the engineering stress above, $a_1 - a_4$ ; $b_1 - b_4$ and $c_1 - c_2$ are constant material parameters. The best-fit parameters to the PTFE and PVC test can be found in Table 2. $a_1$, $a_2$, $b_1$, $b_2$, and $c_1$ determine the asymptote of the exponential functions, so by neglecting the expressions in the brackets, they represent the linear approximation of the stress-strain relation.

**Table 2.** Best-fit parameter values of the two tested materials

| Materials | Linear parameters | | | | Nonlinear parameters | | | | Interaction parameters | |
|---|---|---|---|---|---|---|---|---|---|---|
| | $a_1$ | $a_2$ | $b_1$ | $b_2$ | $a_3$ | $a_4$ | $b_3$ | $b_4$ | $c_1$ | $c_2$ |
| Verseidang Duraskin B 18089[2] | 7.11 | 6.97 | 1.51 | 3.07 | 0.83 | 1.94 | 0.27 | 0.73 | 0.54 | 0.34 |
| **Sauleda Monza Polyester AT 1100** | 6.00 | 11.00 | 1.86 | 1.50 | 0.082 | 0.101 | 0.12 | 0.008 | 0.005 | 0.77 |

The first two exponential components are derived from the elongation of yarns during the tension. The third term shows the interaction between the yarns based on the phenomenon that every elastic constitutive law should satisfy the energy conservation criteria:

$$\frac{\partial \sigma_w}{\partial \varepsilon_f} = \frac{\partial \sigma_f}{\partial \varepsilon_w} = 2c_1 c_2 (\varepsilon_w \varepsilon_f)^{2c_2} + c_1 (\varepsilon_w \varepsilon_f)^{2c_2} \tag{3}$$

Engineering stress and Biot strains were used for acquiring an accurate result during the parameter identification. Figures 1 to 4 show the normal stress-strain diagrams in the weft and warp directions, respectively, of the parameter fitting for the PVC coated polyester fibre material with the existing model. The fitting procedure was running for the three sets of the measurements (warp, weft, and biaxial) simultaneously so that the represented functions cover the bi-axial behavior of the material.
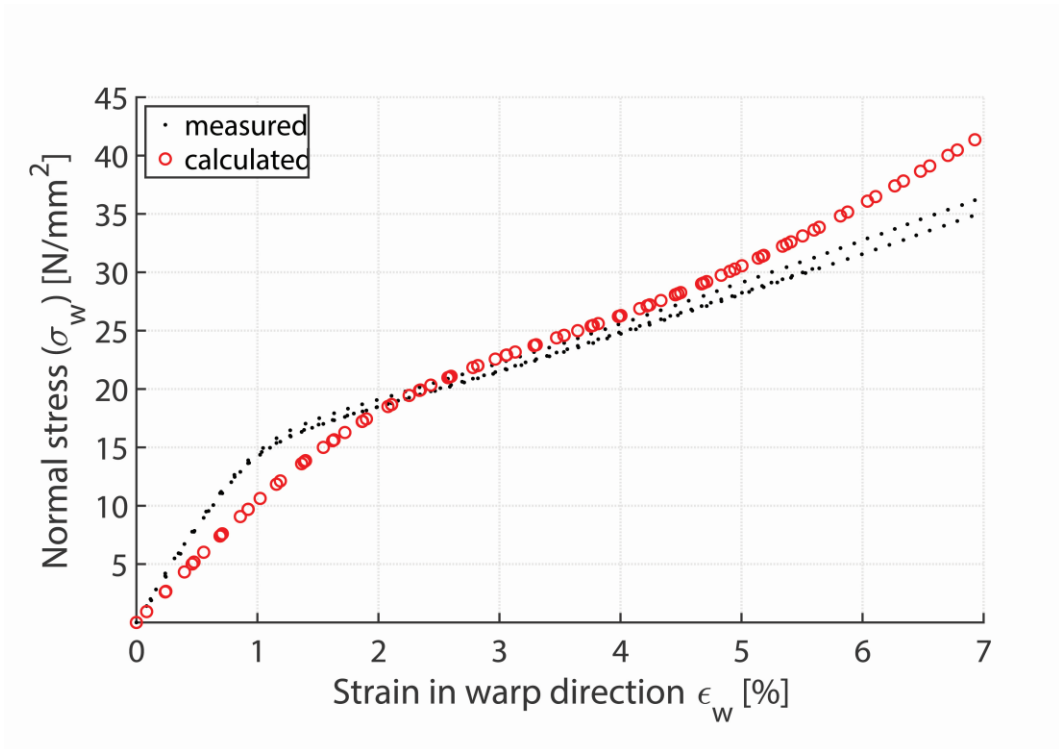
**Figure 1.** The uniaxial projection of the result of the parameter identification for the warp direction for PVC coated textile.
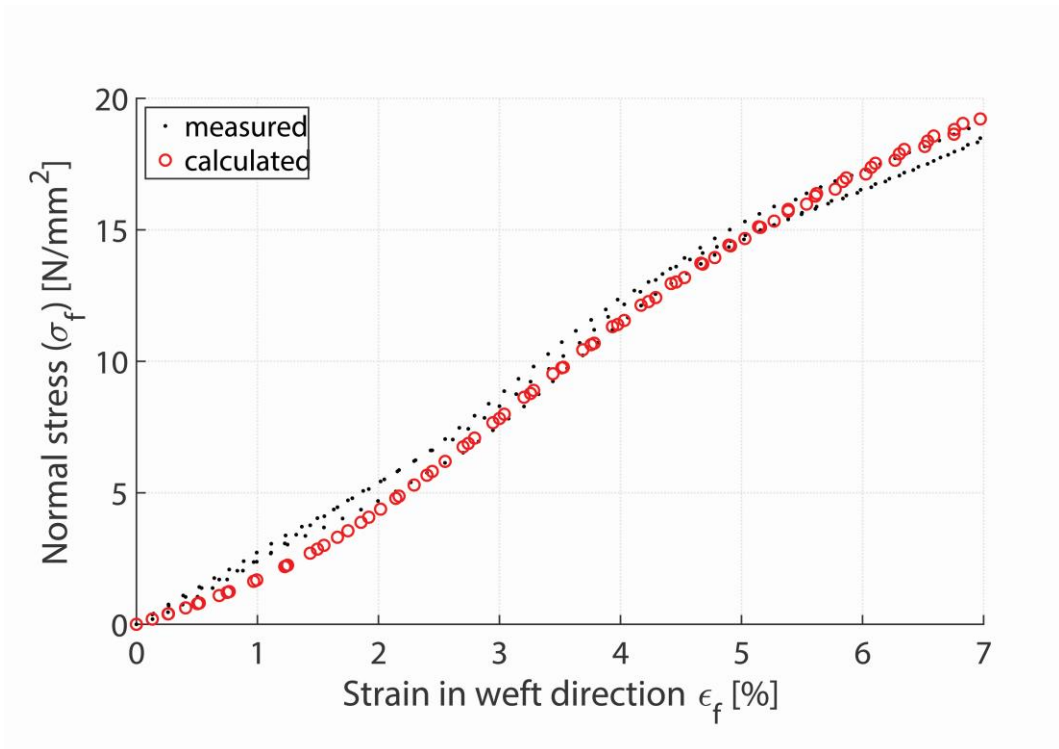


**Figure 2.** The uniaxial projection of the result of the parameter identification for the weft direction for PVC coated textile.
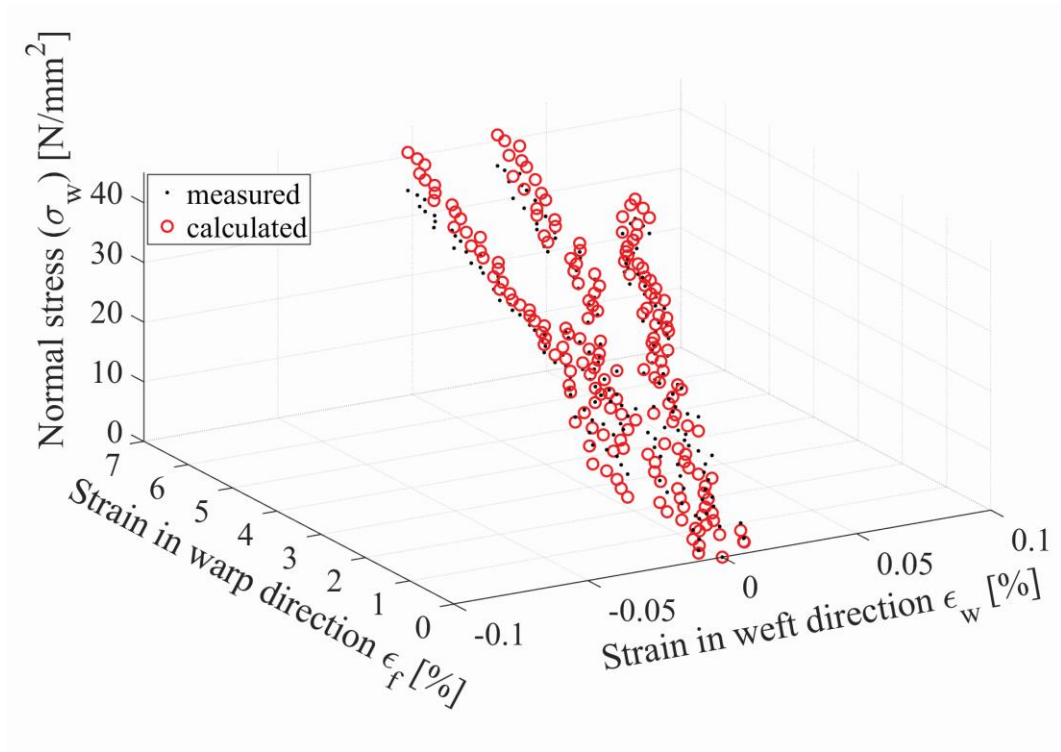
**Figure 3.** The representation of the result of the parameter identification for the warp stress direction by the function of the bi-axial strains.
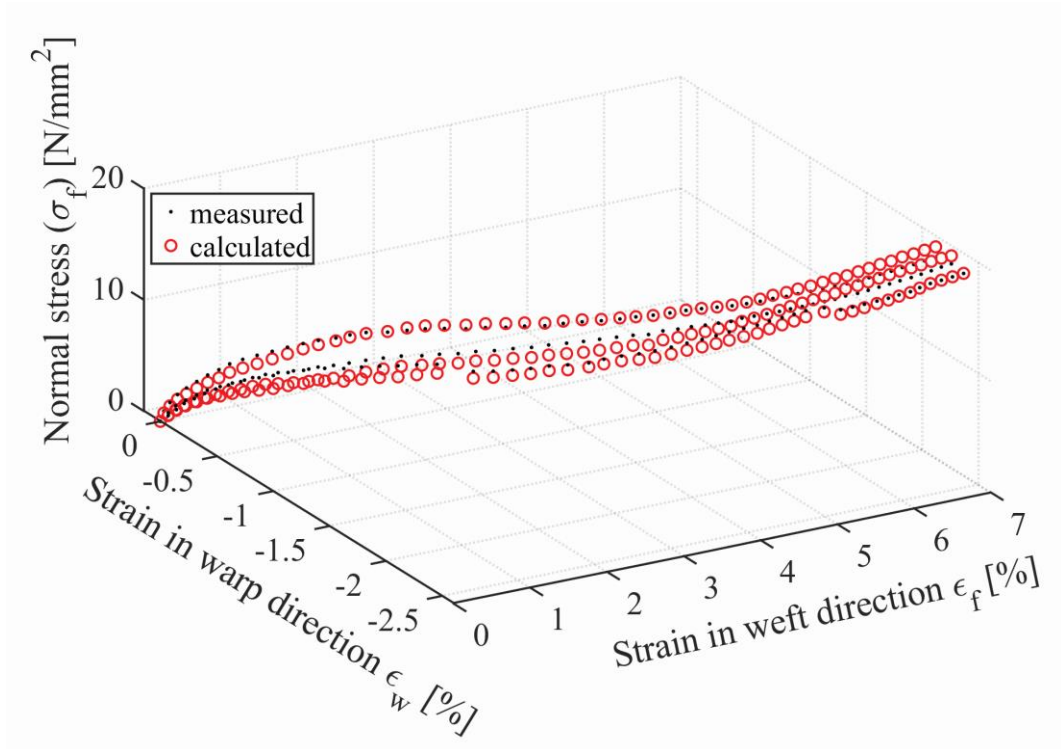


**Figure 4.** The representation of the result of the parameter identification for the weft stress direction by the function of the bi-axial strains.

The method of parameter identification is given in paper[2] in detail. For the parameters in the exponential terms, the variable projection method[1,19], implemented in MATLAB, seemed to be the best choice. For the parameters in the interaction term, a least square minimization proved to be appropriate. The

determination of the coefficient for the fit was $R^2 = 0.980$. Table 3. shows the accepted range of the parameter identification for the PVC material based on the realistic expectation based on datasheet of manufacturers and the analysis of the exponential functions with the acquired data.

**Table 3.** The plausible ranges of the model parameters:

|  | min | max |
|---|---|---|
| Linear parameters | | |
| $a_1$ | 5 | 10 |
| $a_2$ | 10 | 15 |
| $b_1, b_2$ | 1.5 | 2.5 |
| Nonlinear parameters | | |
| $a_3, a_4$ | 0 | 0.2 |
| $b_3, b_4$ | 0 | 1 |
| Interaction parameter | | |
| $c_1$ | -1 | 5 |
| $c_2$ | 0 | 1 |

For the Total Lagrange Method (TLM), the secant of the stress-strain curve should be used during the nonlinear structural analysis. The stiffness matrix is diagonal because the transversal deformation is considered in the calculation of the secants. It reads

$$D = \begin{bmatrix} \frac{\sigma_w}{\varepsilon_w} & 0 & 0 \\ 0 & \frac{\sigma_f}{\varepsilon_f} & 0 \\ 0 & 0 & G \end{bmatrix}. \tag{4}$$

For the case of the Updated Lagrange Method (ULM) the tangential stiffness matrix is suitable, i.e.,

$$D = \begin{bmatrix} \frac{\partial \sigma_w}{\partial \varepsilon_w} & \frac{\partial \sigma_f}{\partial \varepsilon_w} & 0 \\ \frac{\partial \sigma_f}{\partial \varepsilon_w} & \frac{\partial \sigma_f}{\partial \varepsilon_f} & 0 \\ 0 & 0 & G \end{bmatrix}. \tag{5}$$

To obtain a proper model of the shear behavior, additional experiments are needed. This paper is meant to make this development.

## 3. Model development

To introduce a proper shear function, the shear behavior of technical textiles is studied. Note that there is no standardized experimental method to capture the shear deformations[20]. One may use frame devices for producing pure shear in a technical textile sample. Some tests use the bias test method (uniaxial test), where subtle mechanical calculations are required. During a test, a locking effect often occurs between the yarns over a certain level of the deformation, affecting the further relative displacement of the orthogonal yarns, thus the shear behavior in the beginning. For further analysis in the present phenomenological model, the locking

effect and the flexural stiffness of the yarns are not separated from the shear strains. Furthermore, the analysis is limited to the region where 4-5% of the normal strain diagram's initial slope occurs. Simple uniaxial tension tests were carried out as before, but with a varied orientation of the yarns to cause normalized shear effect in the center of the test specimen[21].

### 3.1. Experimental arrangements

To express the shear function, both the shear stress and the shear deformation should be measured. Seven uniaxial test series were carried out, where each series consisted of three specimens. In each series, the yarns had an angle ($\varphi$) to the tensile force's direction between 0-90° in 15° steps. (Figure 5).
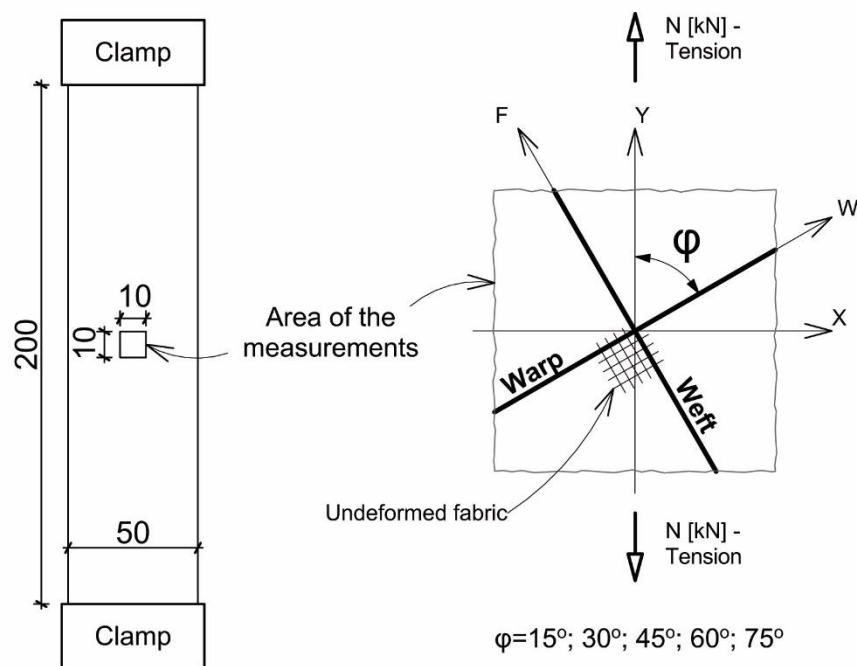


**Figure 5.** The experimental arrangement of the test strips

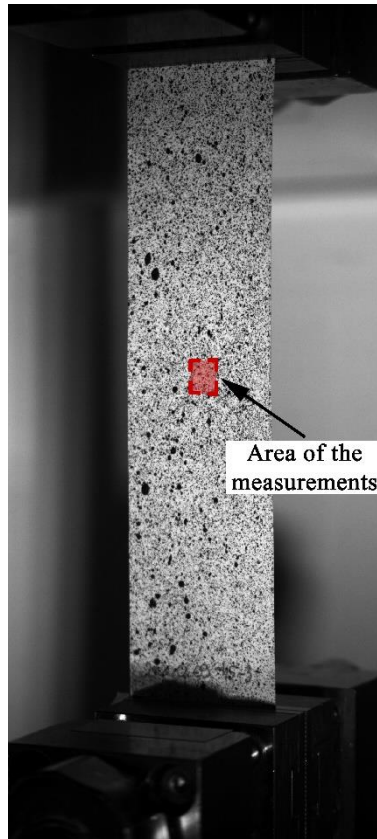**Figure 6.** A photo about the test strip $\varphi = 45°$

The material of all the specimens was PVC coated polyester fibre (Tab. 2). Each test strip was cut with a width of 50 mm, and the grip distance was 200 mm. The displacement tests were carried out with a tensile test machine Zwick Z020. The speed of elongation was 0.20 mm/s. Each specimen was prestressed between 20-40 N to eliminate the waving at the edges that resulted from the storage. The test terminated at the failure of the specimen. To record the strain data, a Messphysik ME-46 full image video-extensometer was used in each series. The recordings were carried out with a set of stereo cameras due to the waving occurrence. The recorded data was processed by the software Mercury RT® (version 2.7). A line probe was defined by two end points (control points) in the yarn direction inside a 10 by 10 mm square on the middle of the specimen. During the test, the average elongation of the line probe and its average angle change to the horizontal axis of the original configuration was measured. The data was calculated by the following correlation settings: 0.2 px correlation interval, 41x41 px template height width 4 control points, fast speed, and high correlation quality (Figures 6-8). Although the Mercury RT® can express deformation tensors, only with one camera measurement, not with a stereo camera. As the surface of the specimen slightly wrinkles during the test, the measurement cannot be accurate with a single camera, so the line probe method should be chosen as described above.
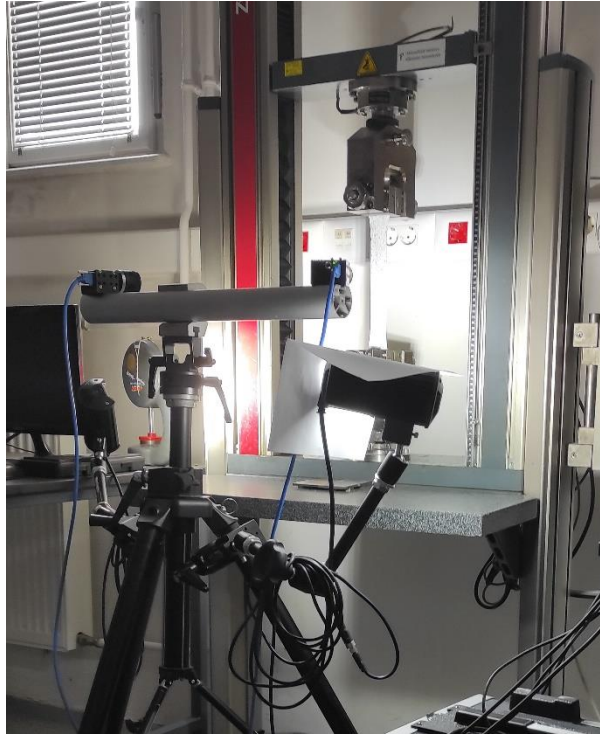
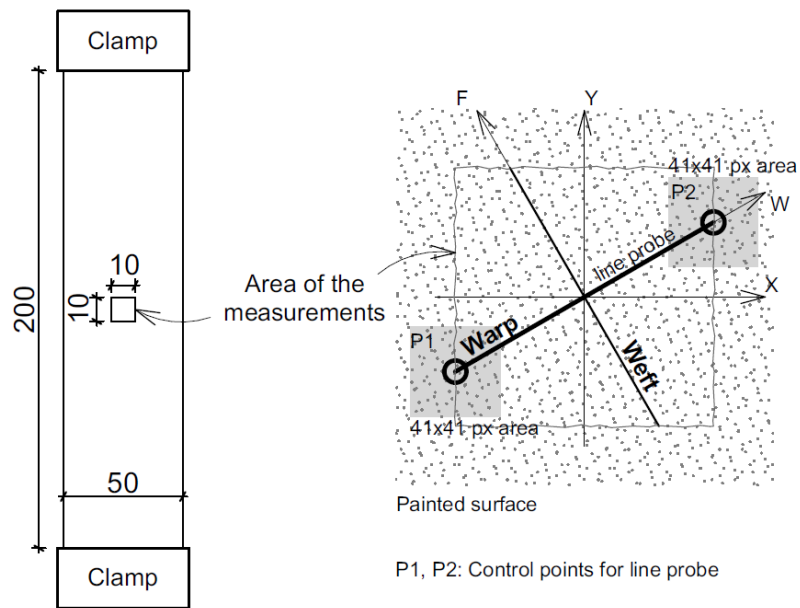**Figure 7.** The test configuration with equipment



**Figure 8.** The defined line probe and correlation interval area around its control points.

### 3.2. Stress-strain calculation

During the measurements, the machine's tension force and strains of the specimen were registered in the loading plane. The fabric material was considered a continuum with sole in-plane deformation modes, namely in-plane elongation and in-plane shear[13]. In this plane, two orthogonal frames were defined. In the "*xy*" *system*, the *y*-axis was parallel to the axis of the loading direction, and the *x*-axis was orthogonal (Figure 5). However, for supplementing the material law, the stress-strain diagram should be expressed in the frame of the textile yarns. The plane determined by the warp and weft yarns will be called the "*wf*" system for further

analysis. The angle between the *y*-axis of the "*xy*" system and the weft yarn of the "*wf*" system is denoted to φ.

$\mathbf{e}_{w0}$ and $\mathbf{e}_{f0}$ are the initial fiber direction unit vectors for the warp and weft directions, respectively. They are represented in the *"wf"* coordinate system. The deformation gradient tensor reads:

$$\mathbf{F} = \partial \mathbf{x}/\partial \mathbf{x}^{j,0} \otimes \mathbf{i}^j, \tag{6}$$

where $\mathbf{x}^0$ and $\mathbf{x}$ are the coordinates of the initial and actual state, respectively. Here $\mathbf{i}$ is the unit basis vector in the initial frame. Each quantity is represented in the *"xy"* coordinate system. The following tensors are used in the sequel to obtain the strain rates for further investigations:

$$\mathbf{C} = \mathbf{F}^{\mathrm{T}}\mathbf{F}, \tag{7}$$

$$\mathbf{E} = \frac{1}{2}(\mathbf{C} - \mathbf{I}), \tag{8}$$

where $\mathbf{C}$ is the right Cauchy-Green deformation tensor, $\mathbf{E}$ is the Green-Lagrangian strain tensor, and $\mathbf{I}$ is the unit tensor.

The engineering strain tensor components in the yarn directions (warp and weft) and the angle change can be expressed as:

$$\varepsilon_{ww} = \sqrt{\mathbf{e}_{w0}\,\mathbf{C}\,\mathbf{e}_{w0}} - 1, \tag{9}$$

$$\varepsilon_{ff} = \sqrt{\mathbf{e}_{f0}\,\mathbf{C}\,\mathbf{e}_{f0}} - 1, \tag{10}$$

$$\gamma_{wf} = \sin^{-1}\frac{2\mathbf{e}_{w0}\mathbf{E}\mathbf{e}_{f0}}{(1+\varepsilon_{ww})(1+\varepsilon_{ff})}. \tag{11}$$
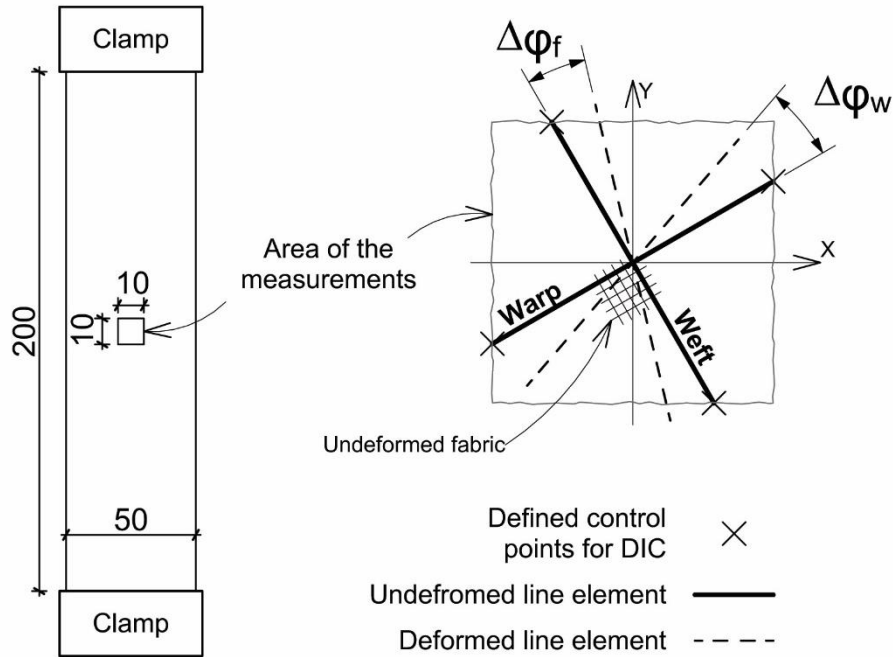


**Figure 9.** The measured strains for the determination of the shear modulus during the test.

The determination of the components of the strain tensors was simple due to the application of the video extension meter. The normal strains ($\varepsilon_{ww}$, $\varepsilon_{ff}$) in the directions of yarns are acquired from the instrument directly. The change of line element length was accepted as a strain. The angle change of the line elements parallel to the warp and weft yarns was monitored to the direction $x$ of the original configuration ($\Delta\varphi_w$, $\Delta\varphi_f$) (Fig. 9). The engineering shear strain is calculated from the following equation:

$$\gamma_{wf} = \Delta\varphi_w + \Delta\varphi_f. \tag{12}$$

The engineering strain tensor of the surface in the *"wf"* system is obtained via:

$$\boldsymbol{\varepsilon} = \begin{bmatrix} \varepsilon_{ww} & \frac{1}{2}\gamma_{wf} \\ \frac{1}{2}\gamma_{wf} & \varepsilon_{ff} \end{bmatrix}. \tag{13}$$

During the tests, the tension force of the machine was measured, from which a normalized tensile stress $\sigma_{yy}$ can be expressed using the geometry of the original cross-section. The relatively small thickness of the material results in a 2D plane-stress condition, where the out-of-plane normal stress and shear stresses vanish. Furthermore, the stress in the orthogonal $x$-direction is always zero in the uniaxial tests ($\sigma_{xx} = 0$) as the shear stress vanishes, too ($\tau_{xy} = 0$). The stress tensor is a 2nd rank tensor in both coordinate systems (equations 14, 17), which equals the Biot stress in the "$xy$" (reference coordinate) system:

$$\mathbf{T}_{Bxy} = \begin{bmatrix} \sigma_{xx} & \tau_{xy} \\ \tau_{xy} & \sigma_{yy} \end{bmatrix} = \begin{bmatrix} 0 & 0 \\ 0 & \sigma_{yy} \end{bmatrix}. \tag{14}$$

To obtain the stress tensor in the "*wf*" *system* from the stresses in the *"xy"* system, the **Q** transformation matrix is introduced:

$$\mathbf{Q} = \begin{bmatrix} \cos\varphi & \sin\varphi \\ -\sin\varphi & \cos\varphi \end{bmatrix}, \tag{15}$$

where $\varphi$ is the angle of rotation between the *"x"* and the *"w"* or the *"y"* and "*f*" directions. Hence,

$$\mathbf{T}_{Bwf} = \mathbf{Q} \cdot \mathbf{T}_{Bxy} \cdot \mathbf{Q}^{T}, \tag{16}$$

$$\mathbf{T}_{Bwf} = \begin{bmatrix} \sigma_{ww} & \tau_{wf} \\ \tau_{wf} & \sigma_{ff} \end{bmatrix}, \tag{17}$$

where $\sigma_{ww}$ and $\sigma_{ff}$ are the engineering normal stress components in the warp and weft yarns, respectively and $\tau_{wf}$ are the engineering shear stress components.

# 4. The new shear model

### 4.1. Uniaxial shear behavior in the warp-weft plane

From the stress-strain transformations, the elongation and the angle of the yarns were not constant, so shear occurs in the material. In all measurement where $0° < \varphi < 90°$ the engineering stress where expressed by the original area of the section

of the specimen. Figures 10-11 shows the results of the shear stress-strain diagram for each tested angle.
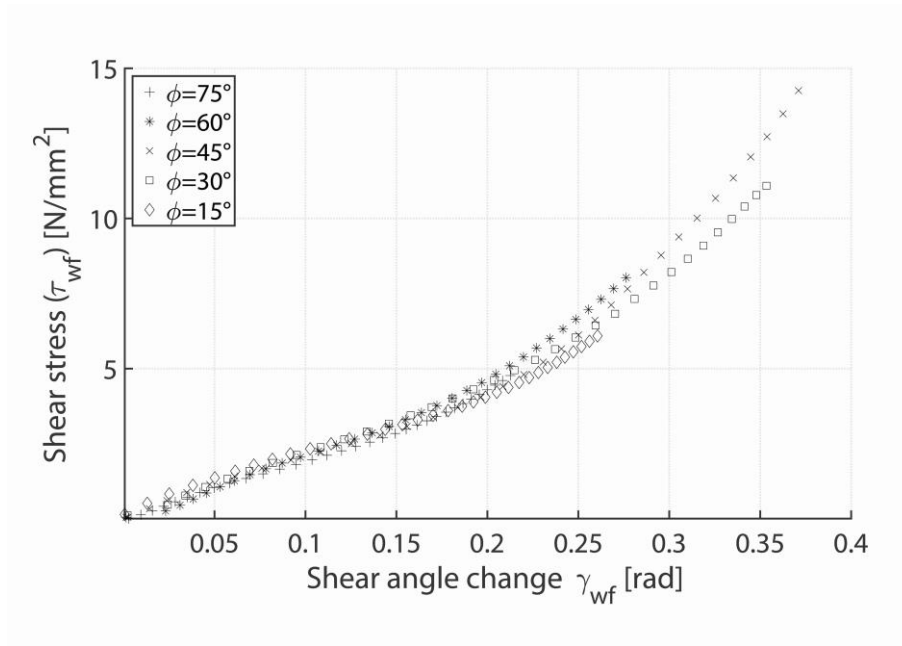


**Figure 10.** The projection of one measured shear stress-strain curves from each load directions projected to the $\gamma_{wf} - \tau_{xy}$ coordinate system.
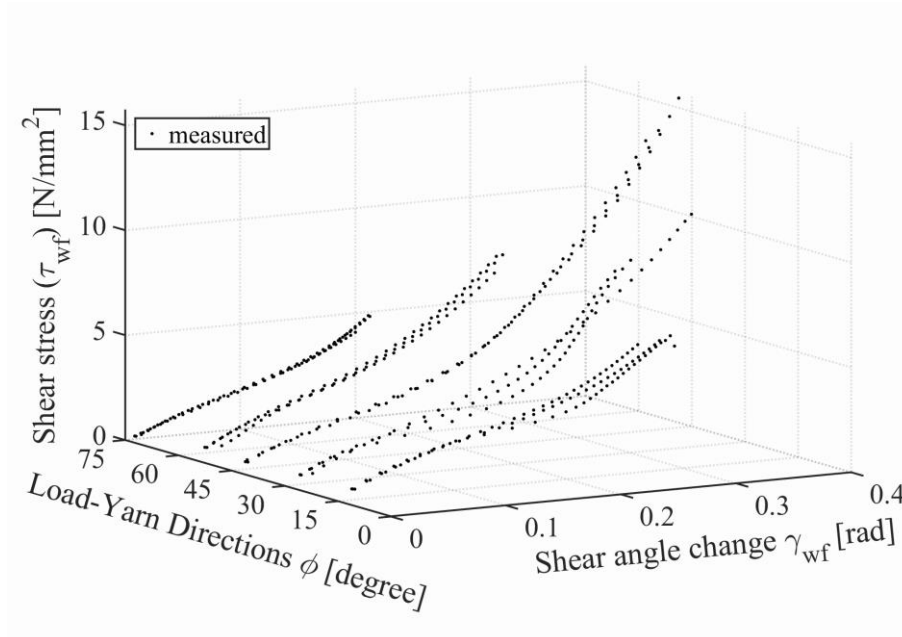


**Figure 11.** The measured stress-strain curves for shear with respect to the angle of the load (φ) in the $\gamma_{wf} - \tau_{xy} - \varphi$ coordinate system.

Based on the shear stress-strain curves, the orthotropic material behavior is the right assumption for the material. The curves do not vary significantly with respect to the tension angle φ, which means that the shear deformation is uncoupled from the yarn elongations. Secondly, the characteristic of the measured values shows a typical feature for technical textiles as it was experienced before[2], where the stress-strain relationship can be described with the two exponential terms effectively in the range

14

of plausible normal strain from an engineering point of view. The shear stress-strain behavior is given with the same idea:

$$\tau_{wf} = d_1 \gamma_{wf} \left( 1 - e^{-d_3 \gamma_{wf}^2} \right) + d_2 \gamma_{wf} \left( e^{-d_4 \gamma_{wf}^2} \right),$$ (18)

where $\tau_{wf}$ $\left[ \frac{N}{mm^2} \right]$ is the shear stress and $\gamma_{wf}$ [rad] is the shear strain between the two yarns. $d_1$; $d_2$; $d_3$; $d_4$ are material parameters, with $d_1$; $d_2$ in $\left[ \frac{N}{mm^2} \right]$ and $d_3$; $d_4$ without dimension.

It is important to note that this paper does not systematically examine the tensile and shear strength of the material. However, all tests were terminated at failure of the material, which occurred close to the upper clamping of the test specimen. The higher the difference from the load angle was, the earlier the crack evolved (Figures 11). For further analysis and parameter identification, the interval $\gamma_{wf} = 0 - 0.25$ rad was taken into consideration (Figures 12).

### 4.2. Parameter identification

The implemented MATLAB method in paper [2] is applied. The variable projection method[1] is a perfect tool to obtain the four parameters of the exponential functions. In the least square minimization, the parameters can suffer a significant shift in the parameter space due to the exponentials' presence in the objective function. However, the variable projection method determines all the linear and nonlinear parameters of the model's exponentials reasonably. The two-input functions for our program consisted of equation (18) of the parameter fitting about the shear the second one consisted the measured stress values ($t_{wf}$) from the experiments. The method found the minimal deviation between the two sets of points, so the parameters for our model.
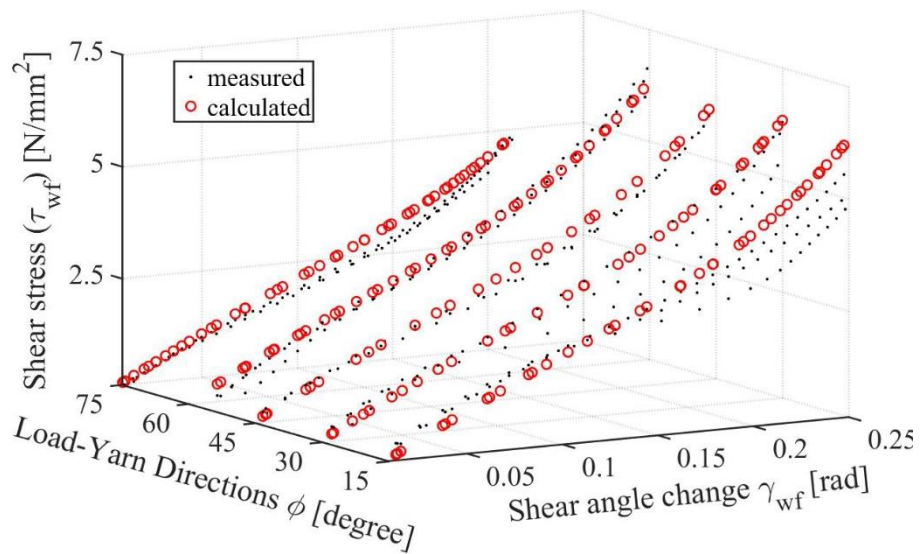


**Figure 12.** The measured and fitted $\tau_{wf}$ shear stress values in function of $\gamma_{wf}$ and φ, ($R^2 = 0.977$ )

The best-fit parameters for the material measured in the shear experiments are: $d_1 = 175$ ; $d_2 = 22.5$ ; $d_3 = 1.91$ ; $d_4 = 21.82$ at the value for the coefficient of determination of the fitness is 0.977. Figure 12. represent the stress-strain curve results of the parameter fit for the uniaxial measurements. Table 4. shows the accepted range for the fitting based on the realistic expectation and the exponential function analysis.

**Table 4.** Range of plausible parameters of the model:

|  | min | max |
|---|---|---|
| Linear parameter: $d_1$ | 150 | 200 |
| Linear parameter: $d_3$ | 5 | 40 |
| Nonlinear parameter: $d_2$ | 1 | 3 |
| Nonlinear parameter: $d_4$ | 0 | 40 |

# 5. Discussion and verification

### 5.1. Stability of the stiffness matrix

Further essential criteria for a stable constitutive material law is to have a positive definite stiffness matrix.

In the case of the supplemented symmetric stiffness matric in TLM is:

$$D = \begin{bmatrix} D_{ww} & 0 & 0 \\ 0 & D_{ff} & 0 \\ 0 & 0 & G \end{bmatrix} = \begin{bmatrix} \dfrac{\sigma_w}{\varepsilon_w} & 0 & 0 \\ 0 & \dfrac{\sigma_f}{\varepsilon_f} & 0 \\ 0 & 0 & \dfrac{\tau_{wf}}{\gamma_{wf}} \end{bmatrix} > 0, \tag{19}$$

Here, it is necessary to verify only that all the main diagonal entries are positive. The opposite is possible only if the divisor and the dividend in one entry has different signs. As it is physically impossible, e.g., positive stress (tension) will not result in negative strains (compression) in any direction. So, the inequality in eq. (19) holds.

In the case of the supplemented symmetric stiffness matric in the ULM reads:

$$D = \begin{bmatrix} D_{ww} & D_{wf} & 0 \\ D_{wf} & D_{ff} & 0 \\ 0 & 0 & G \end{bmatrix} = \begin{bmatrix} \dfrac{\partial \sigma_w}{\partial \varepsilon_w} & \dfrac{\partial \sigma_f}{\partial \varepsilon_w} & 0 \\ \dfrac{\partial \sigma_f}{\partial \varepsilon_w} & \dfrac{\partial \sigma_f}{\partial \varepsilon_f} & 0 \\ 0 & 0 & \dfrac{\partial \tau_{wf}}{\partial \gamma_{wf}} \end{bmatrix} > 0, \tag{20}$$

where D is the stiffness matrix of the material in one step of an Updated Lagrangian type analysis (Eq. 5), $D_{ww}$, $D_{ff}$, $D_{wf}$ and G are the elements of the stiffness matrix for normal stress, transversal effect, and shear, respectively. $G = \dfrac{\partial \tau_{wf}}{\partial \gamma_{wf}}$ is positive in the determined range, see Figure 13.
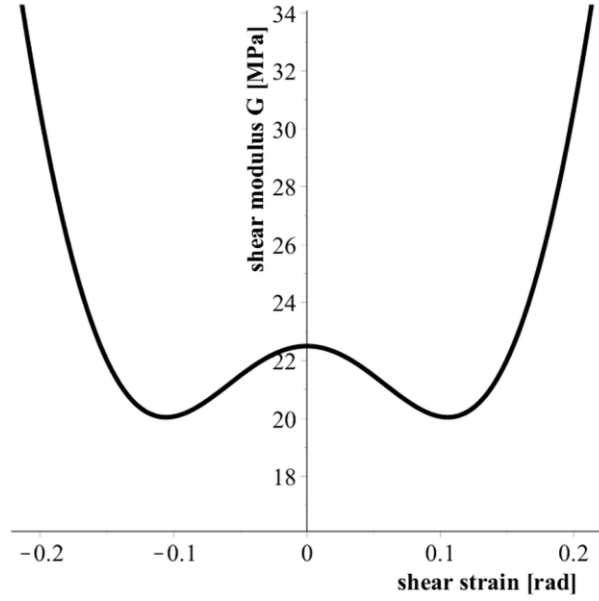
**Figure 13.** The value of the shear modulus in the examined range of shear strains.

When $G$, $D_{ww}$ and $D_{ff}$ are positive according to Eq. 1, 2 and 18 and Tab. 3, it is necessary to verify only that the $D_{3,3}$ minor of the $D$ matrix is positive.

$$D_{3,3} = \frac{\partial \sigma_w}{\partial \varepsilon_w} \frac{\partial \sigma_f}{\partial \varepsilon_f} - \left(\frac{\partial \sigma_f}{\partial \varepsilon_w}\right)^2 \tag{21}$$

With the identified parameters, the function $D_{3,3}$ is a two-variable function of the strains. The surface is above 0 for reasonable stains (the strains are represented in percentage, and the strain is generally under 4-5% even in the ultimate load level).
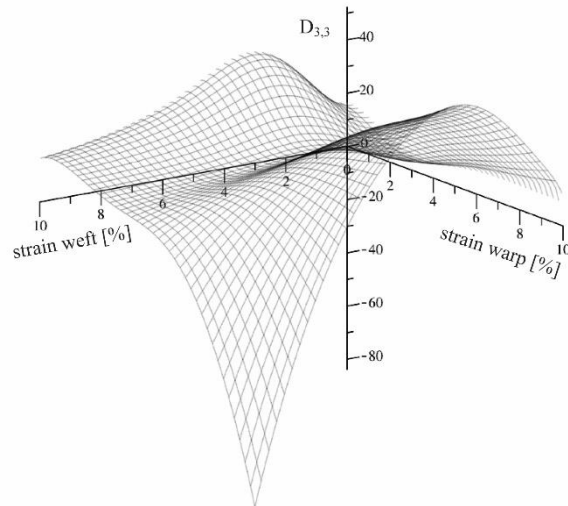


**Figure 14.** The surface of the $D_{3,3}$ function over the space spanned by the strains.
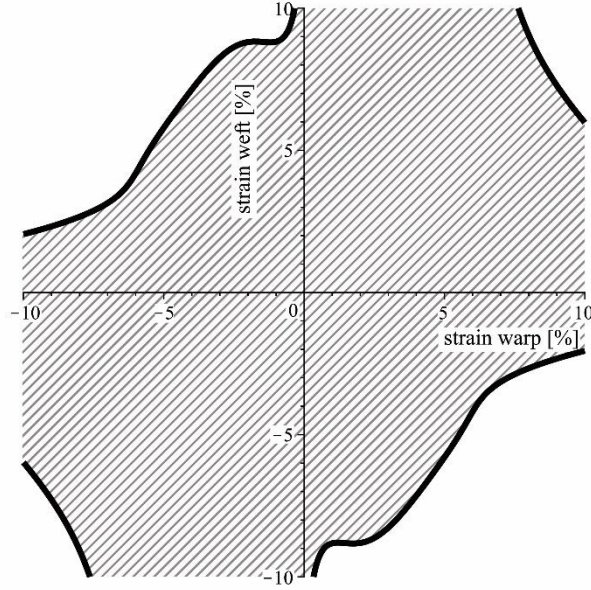
**Figure 15.** The level set of the $D_{3,3}{}'$ function at $z{=}0$.

At larger strains and in negative strains $D_{3,3}$ is negative. Figure 15. depicts the level-set of $D_{3,3} = 0$ where $D_{3,3}$ is positive in the shaded region. To ensure stability in the numerical analysis, the determinant should be verified, but as it is clear from Figure 14., there is no difficulty up to 5-8% strain levels. Figure 15. makes it clear that we are close to the border of the positive-definite regime along with the negative range of the axes and over 7% of a biaxial elongation. Exceeding the boundary can produce instability in the classical finite element method because the inverse of the stiffness matrix is needed. For extremely large strains, the dynamic relaxation method lends a proper strategy[17,23]. As we demonstrated, for moderate strains, the new constitutive model is numerically stable.

### 5.2. Material objectivity

The material objectivity is a key question: the constitutive laws must be independent of the applied frame. It is essential if large strains and/or deformations are considered.

The presented constitutive law uses the strain measured the change between the initial state and the actual state. The base of the difference is the initial state, so it is described in the initial state, in the so-called Lagrangian form. The stress is measured by the average stress calculated from the force introduced by the test machine. The force is distributed on the initial width of the specimen. This is the so-called engineering stress. The stress state initialized in the measurement in the Sec. 3.2. is the same engineering stress which is sometime called the Biot stress tensor in tensor analysis. To transform the Biot stress from the initial state to the actual state, the following equation can be used[17,24]:

$$\mathbf{T} = \mathbf{F}\mathbf{T}_{\mathrm{B}}\mathbf{R}^{\mathrm{T}}\frac{1}{|\mathbf{F}|}, \tag{22}$$

where $\mathbf{T}$ is the Cauchy-stress tensor (the stress tensor of the current state), $\mathbf{F}$ is the deformation gradient, $\mathbf{R}$ is the rotation tensor and $\mathbf{T}_B$ is the stress tensor in the initial state. The Biot stress tensor is based on the right stretch tensor:

$$\mathbf{U} = \sqrt{\mathbf{C}} . \tag{23}$$

The change of the angle is expressed by the Green-Lagrange strain (Eq. 11):

$$\mathbf{E} = \frac{1}{2}(\mathbf{F}^T\mathbf{F} - \mathbf{I}). \tag{24}$$

All the tensors used to express the Biot-stress, and the transformation in Eq. 22 are objective, i.e. the constitutive law is objective by the usage of Eq. 22.

# 6. Conclusion

An updated elastic constitutive material model is introduced for predicting the stresses of technical textiles. This material law, as an extension of the classical elastic orthotropic material law, takes into consideration of the nonlinear behavior of the yarns and the geometric nonlinearity of the yarns inside the fabric. The nonlinear behavior of the shear stiffness is in focus, as this property of the technical textiles was neglected in the past.

A data acquiring strategy is presented, employing uniaxial tension tests. It is shown that the shear stress curve can be described with exponential functions and the shear stress is dominantly independent of the angle between the load and the yarn.

The new phenomenological constitutive law represents the nonlinearity of both the normal- and shear stiffness. The new constitutive law fulfills the requirements for a real material: existence of a strain energy function, positive definiteness at reasonable strain levels and the material objectivity criterium.

# 7. Declaration of Conflicting Interests

The author(s) declared no potential conflicts of interest with respect to the research, authorship, and/or publication of this article.

# 8. Funding

# 9. References

1. O'Leary DP, Rust BW. Variable projection for nonlinear least squares problems. *Comput Optim Appl* 2013; 54: 579–593.
2. Hegyi D, Halász M, Molnár K, et al. An elastic phenomenological material law for textile composites and it's fitting to experimental data. *J Reinf Plast Compos* 2017; 36: 1343–1354.

3. Lomov SV, Gusakov AV, Huysmans G, et al. Textile geometry preprocessor for meso-mechanical models of woven composites. *Compos Sci Technol* 2000; 60: 2083–2095.

4. Haan SI, Charalambides PG, Suri M. A specialized finite element for the study of woven composites. *Comput Mech* 2001; 27: 445–462.

5. Ballhouse D, Köning M, Kröplin B. A microstructure model for fabric-reinforces membranes based on discrete element modeling. In: *Structural membranes 2005* (eds E Onate and B Kroplin). Stuttgart, Germany, 2-5 October 2005, pp. 255–264. Stuttgart: CIMNE

6. Durville D. Approach of the constitutive material behaviour of textile composites through simulation In: *Structural membranes 2005* (eds E Onate and B Kroplin). Stuttgart, Germany, 2-5 October 2005, pp. 307–316. Stuttgart: CIMNE

7. Ambroziak A, Klosowski P. Nonlinear elastic and rheolgical constitutive modeling of PVC-coated polyester fabric using dense net model In: *Structural membranes 2005* (eds E Onate and B Kroplin). Stuttgart, Germany, 2-5 October 2005, pp. 131–138. Stuttgart: CIMNE

8. Ambroziak A, Kłosowski P. Mechanical properties of polyvinyl chloride-coated fabric under cyclic tests. J Reinf Plast Compos 2014; 33: 225–234.

9. Bridgens BN, Gosling PD. Direct stress–strain representation for coated woven fabrics. Comput Struct 2004; 82: 1913–1927.

10. Bridgens BN, Gosling PD. A Predictive Fabric Model for Membrane Structure Design. In: *Structural membranes 2005* (eds E Onate and B Kroplin). Stuttgart, Germany, 2-5 October 2005, pp. 287–296. Stuttgart: CIMNE

11. Chaboche JL. Constitutive equations for cyclic plasticity and cyclic viscoplasticity. Int J Plast 1989; 5: 247–302.

12. Bodner SR, Partom Y. Constitutive Equations for Elastic-Viscoplastic Strain-Hardening Materials. *J Appl Mech ASME* 1975; 42: 385–389.

13. Charmetant A, Orliac JG, Vidal-Sallé E, et al. Hyperelastic model for large deformation analyses of 3D interlock composite preforms. *Compos Sci Technol* 2012; 72: 1352–1360.

14. Selezneva M, Naouar N, Denis Y, et al. Identification and validation of a hyperelastic model for self-reinforced polypropylene draping. *Int J Mater Form* 2021; 14: 55–65.

15. Peng X, Guo Z, Du T, et al. A simple anisotropic hyperelastic constitutive model for textile fabrics with application to forming simulation. *Compos Part B Eng* 2013; 52: 275–281.

16. Peng XQ, Cao J. A continuum mechanics-based non-orthogonal constitutive model for woven composite fabrics. *Compos Part Appl Sci Manuf* 2005; 36: 859–874.

17. Hegyi D. *The analysis of membrane structures and structural membranes by numerical and experimental methods (in Hungarian)*. PhD Thesis, Budapest University of Technology and Economics, Hungary, 2006.

18. Bakonyi P, Halász M, Molnár K, et al. Developement of a biaxial tensile grip for cyclic tensile tests of flexible technical textiles. In: *5th edition of the international conference on intelligent textiles & mass customiztaion* (eds M Lahlou and V Koncar), Casablanca, Morocco, 4-6 November 2015; p8. Casablanka: ESITH

19. Golub GH, Pereyra VD. Separable nonlinear least squares: the variable projection method and its applications. *Inverse Prob* 2003; 19: R1-R26

20. Rothe S, Wendt E, Krzywinski S, et al. Investigation of Shear-Induced Deformation of Reinforcing Textiles by Optical Measurement Devices. Materials 2019; 12: 1029.

21. Cao J, Akkerman R, Boisse P, et al. Characterization of mechanical behavior of woven fabrics: experimental methods and benchmark results. *Compos Part A Appl Sci Manuf* 2008; 39: 1037–1053.

22. Hill R. On constitutive inequalities for simple materials—*I. J Mech Phys Solids* 1968; 16: 229–242.

23. Hegyi D, Sajtos I, Geiszter G, et al. Eight-node quadrilateral double-curved surface element for membrane analysis. Comput Struct 2006; 84: 2151–2158.

24. Basar Y, Weichert D, Nonlinear Continuum Mechanics of Solids. Aachen: Springer, 2000.